

Electrochemical Corrosion Behavior of Spray-Formed Boron-Modified Supermartensitic Stainless Steel



GUILHERME ZEPON, RICARDO P. NOGUEIRA, CLAUDIO S. KIMINAMI, WALTER J. BOTTA, and CLAUDEMIRO BOLFARINI

Spray-formed boron-modified supermartensitic stainless steel (SMSS) grades are alloys developed to withstand severe wear conditions. The addition of boron to the conventional chemical composition of SMSS, combined with the solidification features promoted by the spray forming process, leads to a microstructure composed of low carbon martensitic matrix reinforced by an eutectic network of M_2B -type borides, which considerably increases the wear resistance of the stainless steel. Although the presence of borides in the microstructure has a very beneficial effect on the wear properties of the alloy, their effect on the corrosion resistance of the stainless steel was not comprehensively evaluated. The present work presents a study of the effect of boron addition on the corrosion resistance of the spray-formed boron-modified SMSS grades by means of electrochemical techniques. The borides fraction seems to have some influence on the repassivation kinetics of the spray-formed boron-modified SMSS. It was shown that the Cr content of the martensitic matrix is the microstructural feature deciding the corrosion resistance of this sort of alloys. Therefore, if the Cr content in the alloy is increased to around 14 wt pct to compensate for the boron consumed by the borides formation, the corrosion resistance of the alloy is kept at the same level of the alloy without boron addition.

DOI: 10.1007/s11661-017-3980-6

© The Minerals, Metals & Materials Society and ASM International 2017

I. INTRODUCTION

STAINLESS steel is widely used in the oil industry due to its corrosion resistance properties linked with appropriate mechanical properties. The supermartensitic stainless steel (SMSS) grades, or super 13Cr martensitic stainless steel, have increasingly been used in seamless pipes for drilling, casing, and tubing subjected to application in the corrosive environments of oil and gas fields. Such stainless steel grades are based on the Fe-Cr-Ni-Mo system with up to 13 wt pct Cr, 4–6 wt pct Ni, 0.5 to 2.5 wt pct Mo, low amounts of carbon, nitrogen, phosphorus, and sulfur ($C \leq 0.02$ wt pct, $N, P, S \leq 0.03$ wt pct). SMSS grades are divided into three classes: Low alloy SMSS (11Cr-2Ni); Medium alloy SMSS (12Cr-4.5Ni-1.5Mo); and High alloy SMSS (13Cr-6Ni-2.5Mo).^[1] The optimized microstructures of these alloys are free from δ -ferrite and offers good corrosion resistance in environments containing CO_2 and H_2S .^[2–4] Kondo *et al.*

have studied the corrosion resistance of the SMSS grades in chloride medias containing CO_2 (such as seawater in off-shore fields).^[4] However, pipes and pumps used in the exploitation and production of oil, in addition to corrosive environments, are often subjected to extreme wear conditions. In those cases, the application of stainless steels is greatly limited due to their low hardness or poor wear resistance properties. The exploitation of oil in ultra-deep water regions, as in the case of pre-salt fields at the Brazilian coast, has increased the demand of materials comprising both high wear and corrosion resistance.

Based on this scenario, much effort is being devoted to develop materials, which combine the good corrosion resistance of the stainless steel grades with improved wear resistance. Different approaches have been used to increase the wear resistance of stainless steel parts. Nanostructured and amorphous alloys with high wear and corrosion resistance, alloys with high hardness and high fraction of hard intermetallic, and alloys with strain induced phase transformation are some of the approaches used by different researches around the world.^[5–20] In the context of this paper, the approach used is to increase the wear resistance of stainless steel grades through the modification of their chemical composition. Such modification aims to conscientiously induce the formation of hard phases, increasing the wear resistance, while maintaining the corrosion resistance of the stainless steel matrix.

Spray forming is an advanced casting process useful to produce high-alloyed materials, such as AISI D2 and AISI M3 high-alloyed tool steels, with reduced

GUILHERME ZEPON, CLAUDIO S. KIMINAMI, WALTER J. BOTTA FILHO, and CLAUDEMIRO BOLFARINI are with the Departamento de Engenharia de Materiais, Universidade Federal de São Carlos, Rod. Washington Luiz, Km 235, 13565-905, São Carlos, SP, Brazil. Contact e-mail: zepo@ufscar.br RICARDO P. NOGUEIRA is with the University of Grenoble Alpes, LEPMI, 38000 Grenoble, France, and also with the Department of Chemical Engineering, Gas Research Center, The Petroleum Institute, Abu Dhabi, UAE.

Manuscript submitted September 13, 2016.

Article published online January 30, 2017

macrosegregation, fine microstructure, and uniform distribution of carbides and second phases.^[21] Spray forming has been used to develop several materials, such as aluminum alloys (Al-Si, Al-Mg alloys), iron-based alloys (high chromium cast iron and high speed steel), and metal-matrix-composites (MMC's) with improved wear resistances.^[22–26] In all cases, the wear properties are improved by the microstructural refinement and uniformity promoted by the spray forming process. Kasama *et al.* and Matsuo *et al.* showed that sprayed-formed high chromium cast irons present a substantial refinement in the microstructure scale when compared to the same conventionally cast alloy. The presence of fine M_7C_3 type carbides uniformly dispersed in an austenitic/martensitic matrix was effective to improve considerably both the abrasive and the sliding wear resistances.^[24,25] Recently, the development of the spray-formed boron-modified SMSS has been introduced.^[15] The addition of some boron content, ranging from 0.3 to 0.7 wt pct, combined with the solidification features of the spray forming process, leads to a very refined and homogeneous microstructure composed of low carbon martensite and M_2B -type borides. Such borides are present in a continuous eutectic network extended throughout the microstructure. The presence of these borides resulted in an increase of at least tenfold in the wear resistance of the alloy when compared to the conventional SMSS.^[15] Up till now, the focus has been placed on the evaluation of the wear behavior of the spray-formed boron-modified stainless steel grades. However, the corrosion behavior of such modified steels is of concern as it can be affected by the alloy modification. Therefore, this paper presents a study of the electrochemical corrosion behavior of the spray-formed boron-modified SMSS grades.

II. EXPERIMENTAL

A. Spray Forming

Four different compositions of supermartensitic stainless steel modified with boron additions were spray formed. The selected compositions present different chromium and boron contents, namely 12 wt pct Cr-0.3 wt pct B, 12 wt pct Cr-0.5 wt pct B, 12 wt pct Cr-0.7 wt pct B, and 14 wt pct Cr-0.7 wt pct B, hereinafter called as SM-0.3B, SM-0.5B, SM-0.7B, and SM-14Cr-0.7B, respectively. Disks of approximately 250-mm diameter and 15-mm thick were spray formed in a close-coupled spray forming equipment. Commercial supermartensitic stainless steel bars, iron-boron alloy with 16 wt pct boron, iron-molybdenum alloy with 62 wt pct Mo, commercial pure chromium, and nickel were used as raw materials. In each spray forming experiment, approximately 4 kg of raw materials were melted in an induction furnace and spray formed onto a rotating carbon steel disk substrate. N_2 was used as the atomization gas. In all cases, the pouring temperature was 1923 K (1650 °C), the spray distance 460 mm, and the substrate rotation was 45 rpm. The average melt and gas flow rates of all spray forming experiments were

approximately 0.133 and 0.170 kg s⁻¹, respectively, resulting in a gas-to-metal ratio (GMR) of approximately 1.2.

B. Alloys Characterization

The chemical compositions of the spray-formed boron-modified SMSSs were determined by inductively coupled plasma atomic emission spectrometry (ICP-AES), except C and S, which were analyzed by direct combustion. The microstructures were analyzed by optical microscopy (OM) and scanning electron microscopy (SEM) using a FEI Inspect S50 scanning electron microscope. 3HCl:1HNO₃ solution was used as the etching reagent in order to reveal the microstructure. The morphologies of the borides were revealed by deep etching technique using a solution composed of 10 mL HCl, 3 mL HNO₃, 5 mL FeCl₃, and 82 mL ethyl alcohol.

C. Electrochemical Analysis

The working electrodes (WE) were the cross section of cylindrical samples with 13-mm diameter cut by electrical erosion from the SM-0.3, SM-0.5, SM-0.7, and SM-14Cr-0.7B deposits. Spray forming is prone to yield higher porosity levels at the top surface of the deposit. Based on this observation, the top surfaces of the cylindrical deposited samples were polished until the higher porosity region is completely removed (for all samples, removing 2 mm of material was enough to reach the low porosity region, about one percent measured by area fraction). The analysis was performed in the low porosity cross sections with the surfaces polished until #600 grit.

Electrochemical impedance spectroscopy (EIS) and potentiodynamic polarization measurements were performed using a REF600 Gamry potentiostat and a conventional three electrodes set up. A saturated calomel electrode (SCE) and a platinum sheet were used as the reference (RE) and counter-electrode (CE), respectively. The electrolyte was a 35 g/L NaCl solution in deionized water at pH 4.0 (controlled by addition of diluted H₂SO₄). In order to evaluate the effect of boron, three test protocols were designed to study the effect of the variation of chemical composition of the studied materials (mainly in terms of B and Cr contents) on the corrosion resistance of the alloys. The test protocols designed allow the observation of the electrochemical corrosion behavior of the studied alloys under different conditions of passivation, i.e., the designed experiments subjected the samples to passivation in different solutions (more or less oxidizing) for different periods. The designed test protocols are as follows:

- (I) The samples were immersed 24 hours in deionized water for a pre-passivation treatment. After pre-passivation, the sample was transferred to the electrolyte and the open circuit potential (OCP) was measured for one hour. Subsequently, EIS analysis was performed with a potential amplitude of 10 mV around the

OCP value and frequencies varying from 10^5 to 10^{-2} Hz. Since EIS is a non-destructive testing, after the measurement, the sample was kept ten minutes longer in OCP condition and potentiodynamic polarization test was carried out in sequence. The potentiodynamic polarization curves were obtained by sweeping the potential from 50 mV below the corrosion potential (determined by the OCP measurement) to a maximum potential (named critical potential- E_{crit}) corresponding to a current of 0.1 mA cm^{-2} .

- (II) The samples were directly immersed in the electrolyte for one hour of OCP measurements without pre-passivation treatment. Subsequently, the EIS and polarization tests were carried out following the same procedure as described in protocol (I).
- (III) The samples were maintained 12 hours in the electrolyte while measuring the OCP. Subsequently, the EIS and polarization tests were carried out following the same protocol as described in protocol (I). In this case, after EIS measurements the samples were left for 1 hour at OCP before the polarization test.

It must be stressed that the test protocols as described above do not represent any specific condition in terms of application of the alloys in service; however, the designed experiments allow the clearly evaluation of the effect of chemical composition on the corrosion resistance of the alloys.

In order to observe the corroded surfaces of the spray-formed boron-modified SMSSs, samples with polished surfaces were polarized anodically until the current density has reached 5 mA cm^{-2} . Images of the corroded surfaces were captured by optical microscopy technique.

Electrochemical noise (EN) measurements were carried out to evaluate the repassivation kinetics of the spray-formed boron-modified SMSS after a simulated wear event. Similar tests aiming at evaluating the repassivation kinetics of samples after scratching events have been reported in literature.^[27] Two identical samples of the same alloy were connected as CE and WE at the electrochemical cell in a zero resistance ammeter (ZRA) configuration. After assembling the electrochemical cell, the samples were immersed in the electrolyte for 24 hours. The coupling current between both samples was measured during the last hour of immersion before being interrupted. The surface of the sample acting as CE was then abraded through a #240

grit sandpaper for 10 seconds (using a hand drill with constant rotation) simulating an abrasive or wear event upon the metallic surface. Immediately after finishing the abrasion, the coupling current measurement was resumed. The coupling current was recorded for two more hours in order to evaluate the repassivation tendency of the studied alloys.

For comparison, the same electrochemical analysis was carried out in a commercial medium alloy SMSS. Table I and Figure 1 present its chemical composition and microstructure, respectively.

III. RESULTS AND DISCUSSION

The chemical compositions of the SM-0.3B, SM-0.5B, SM-0.7B, and SM-14Cr-0.7B are shown in Table II. The final boron contents of the spray-formed alloys were 0.37, 0.54, 0.69, and 0.71 wt pct, respectively. One can see that the Cr, Ni, and Mo contents of the SM-0.3B and SM-0.7B (11.9-12.0 wt pct Cr, 5.7-5.8 wt pct Ni, and 2.0 wt pct Mo) are within the range of the conventional medium alloy SMSS. The SM-0.5B presents a Cr content of 10.85 wt pct, slightly lower than the Cr content of the conventional low alloy SMSS grade (11.0 wt pct). The lower Cr content presented by the SM-0.5B resulted from incomplete incorporation of the commercial pure chromium during the melting process in the alloy production. On the other hand, the SM-14Cr-0.7B alloy presents a Cr content of about 13.6 wt pct, which is higher than the upper limit

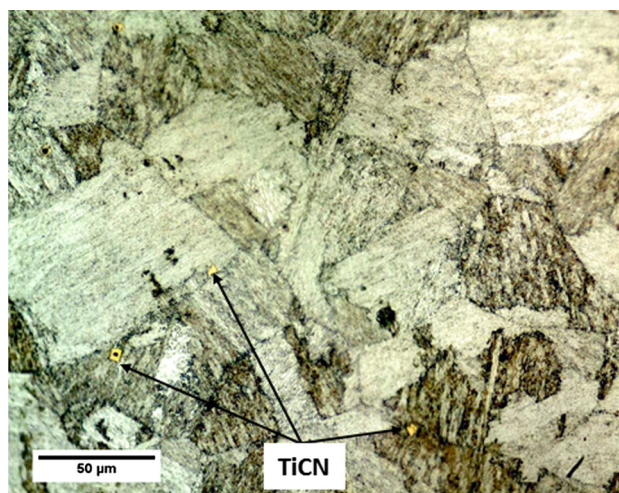


Fig. 1—Microstructure of commercial medium alloy SMSS.

Table I. Chemical Composition of the Commercial Supermartensitic Stainless Steel (Weight Percent)

Pct C	Pct Cr	Pct Ni	Pct Mo	Pct Si	Pct S	Pct P	Pct Mn
0.007	11.86	5.87	2.00	0.25	0.001	0.016	0.45
Pct Nb	Pct W	Pct Co	Pct N	Pct Cu	Pct V	Ti	Pct Fe
0.01	0.01	0.03	0.0095	0.06	0.03	0.135	79.26

Table II. Chemical Composition of the Spray-Formed Boron-Modified Supermartensitic Stainless Steel

Pct wt	Pct C	Pct Cr	Pct Ni	Pct Mo	Pct B	Pct Ti	Pct Mn	Pct S	Pct Fe
SM-0.3B	0.066 ± 0.005	12.00 ± 0.17	5.68 ± 0.03	2.09 ± 0.01	0.37 ± 0.03	0.044 ± 0.004	0.40 ± 0.06	0.0014 ± 0.0001	bal.
SM-0.5B	0.068 ± 0.001	10.85 ± 0.52	5.38 ± 0.25	1.90 ± 0.09	0.54 ± 0.04	0.044 ± 0.004	0.38 ± 0.05	0.0041 ± 0.0001	bal.
SM-0.7B	0.096 ± 0.004	11.88 ± 0.13	5.88 ± 0.03	2.09 ± 0.01	0.69 ± 0.02	0.041 ± 0.006	0.49 ± 0.06	0.001696 ± 0.0003	bal.
SM-14Cr-0.7B	0.039 ± 0.004	13.56 ± 0.26	5.42 ± 0.03	1.82 ± 0.04	0.71 ± 0.08	0.040 ± 0.006	0.52 ± 0.05	0.00151 ± 0.0003	bal.

established for the conventional high alloy SMSS grade. In this case, the higher chromium content was intentionally added, aiming at evaluate the corrosion behavior of a Cr-rich grade of the spray-formed boron-modified SMSS. It is worth noting that the boron-modified alloys presented carbon contents ranging from 0.04 to 0.09 wt pct, which are above the maximum limit established for the conventional SMSS grades (0.03 wt pct); such higher C content of the spray-formed alloys came from impurities of the raw materials, mainly from the iron-boron alloy, which has carbon content of about 0.3 wt pct.

The area porosity fraction of the deposits was determined by automatic image analysis. The porosity fraction measured in case of each of the deposits was lower than 1 pct, which is considerably low for spray-formed alloys. A round pore can be seen in the

microstructure of the SM-0.7B shown in Figure 2(c). This sort of pore is typical of solidification shrinkage porosity, which arises from the volume contraction during solidification. When the processing parameters of spray forming is optimized, the porosity levels caused by other mechanisms such as gas entrapment, and low liquid fraction at the deposition zone (called cold porosity) are minimized. However, the solidification shrinkage porosity is intrinsic to the solidification process and cannot be avoided.

The microstructures of the SM-0.3B, SM-0.5B, SM-0.7B, and SM-14Cr-0.7B are shown in Figure 2. In all cases, the microstructure is composed of martensitic matrix with hard M_2B -type borides at the prior austenite grain boundaries (the phase identification by X-ray diffraction can be found elsewhere^[15]). It can be seen that the increase of boron content from 0.3 to

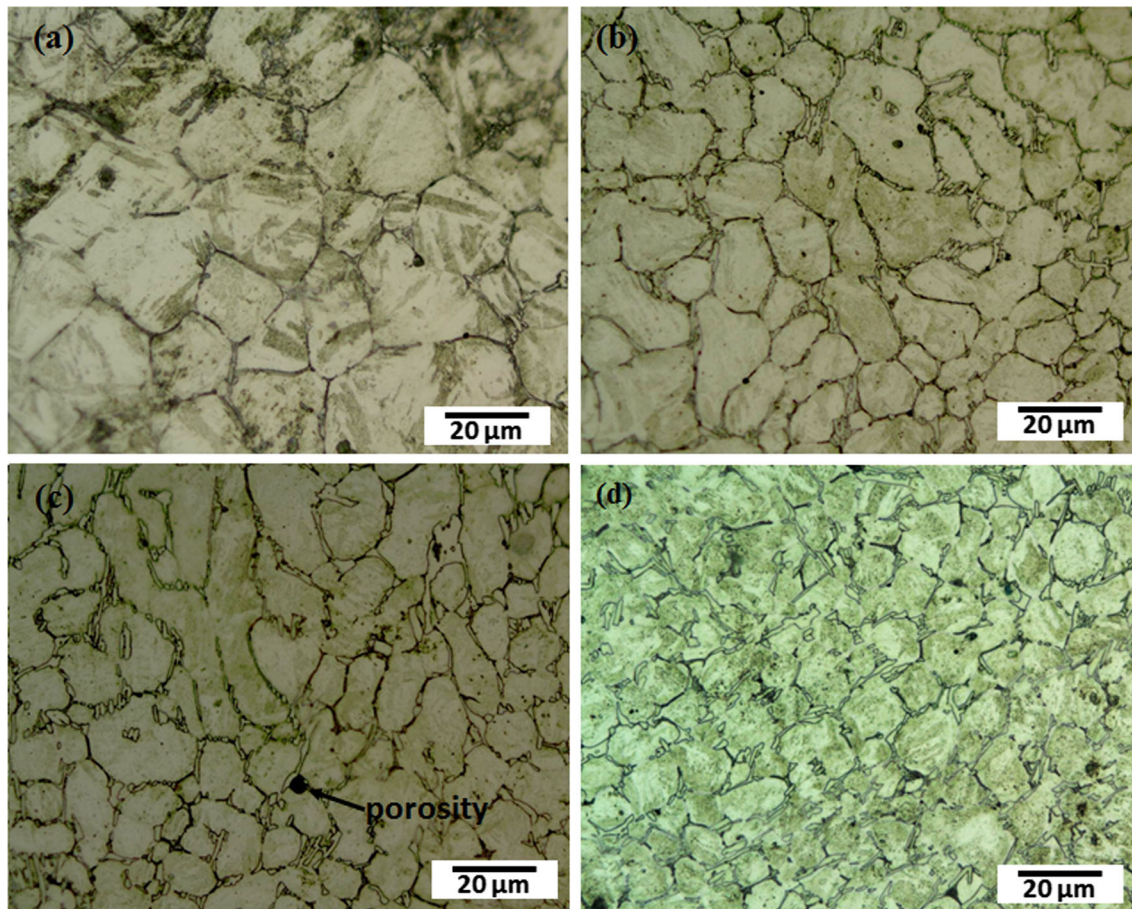


Fig. 2—OM images showing the microstructures of the (a) SM-0.3B, (b) SM-0.5B, (c) SM-0.7B, and (d) SM-14Cr-0.7B. Etching: Vilela.

0.7 wt pct has two important effects: (i) increasing the borides fraction at the grain boundaries and (ii) decreasing the grain size. The average grain sizes of the SM-0.3B, SM-0.5B, SM-0.7B, and SM-14Cr-0.7B are about, 23, 14, 12.5, and 11 μm , respectively. The boride morphologies of the spray-formed boron-modified SMSS are observed in Figure 3. It can be seen that the M_2B -type borides present an interconnected network morphology throughout the microstructure. Such microstructure results from the solidification characteristic of the spray forming process. The four alloys studied here are hypoeutectic with the primary phase being the γ -austenite. With cooling, the primary γ -austenite grows and, since boron has practically no solubility in the steel phase, all boron segregates into the remaining liquid in the deposition zone. When the eutectic temperature is achieved, the eutectic reaction $\text{L} \rightarrow \gamma + \text{M}_2\text{B}$ takes place. Thus, the hard M_2B -type borides are formed in the last stage of solidification generating the continuous eutectic network around the equiaxed primary γ -austenite phase. The formation of equiaxed grains and boride morphology of the

spray-formed boron-modified SMSS was reported previously.^[28] After solidification, the cooling rate of the deposit is sufficient to induce the martensitic transformation of the primary and eutectic γ -austenite.

The microstructure formation may have an important role on the corrosion behavior of the spray-formed boron-modified SMSSs. The addition of 0.3 to 0.7 wt pct of boron to the standard chemical composition of the medium alloy SMSS grade led to the formation of (Fe,Cr)-rich M_2B -type borides by the eutectic reaction $\text{L} \rightarrow \gamma + \text{M}_2\text{B}$. As boron has extremely low solubility in steels (<0.0008 wt pct), all the borides are formed during the solidification process.^[15,28–30] This is important because there is no possibility of further borides precipitation in the matrix after solidification; thus, avoiding the formation of Cr-depleted regions in the vicinity of those precipitates. For instance, since carbon has high solubility in the high-temperature austenite, wear-resistant tool steels such as AISI D2 and AISI M2:3, when spray-formed, present high level of Cr-rich carbides (M_7C_3 or MC) precipitation.^[21,31] Such precipitation can generate critically Cr-poor

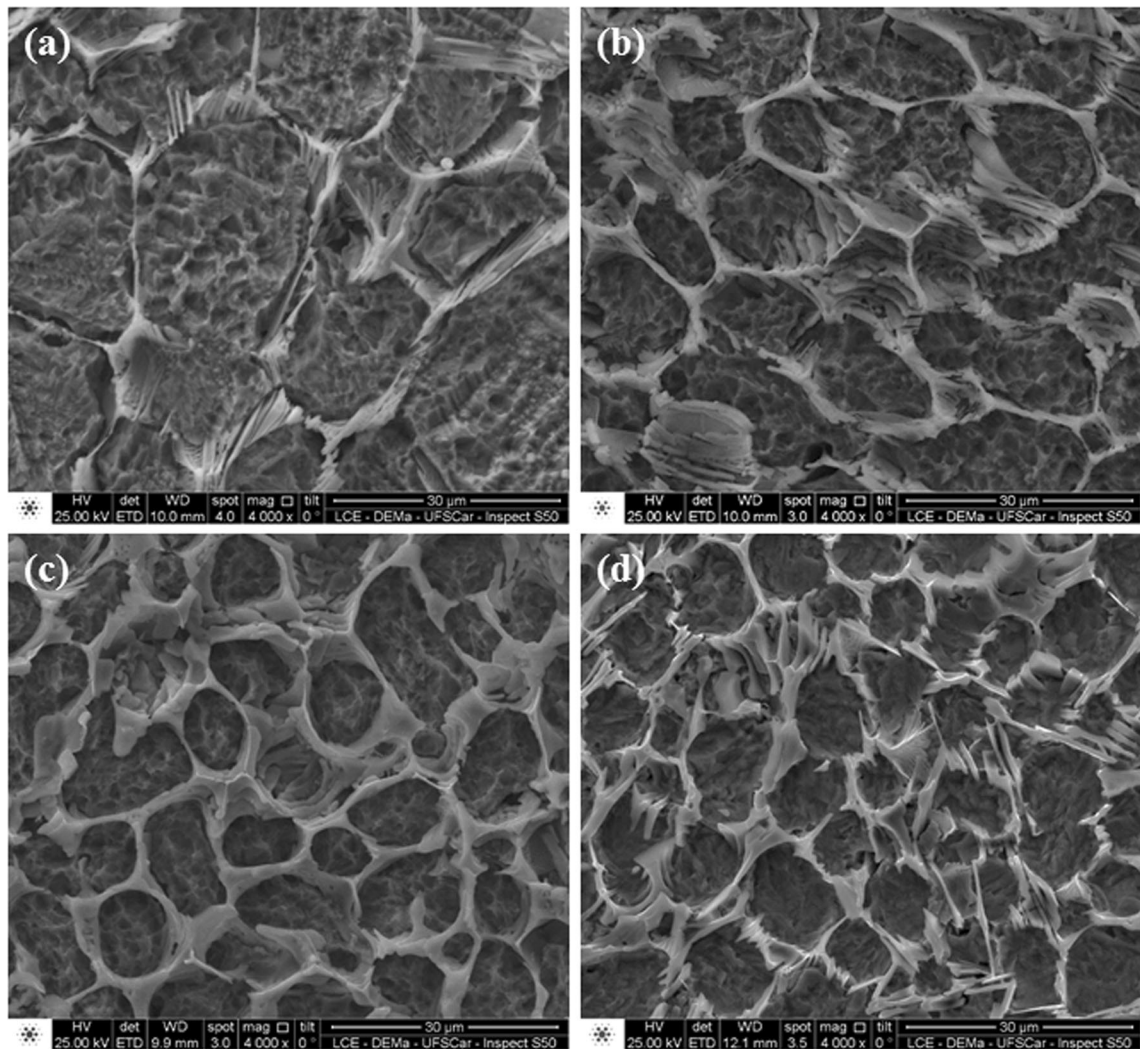


Fig. 3—SEM images showing the M_2B -type borides morphology of (a) SM-0.3B, (b) SM-0.5B, (c) SM-0.7B, and (d) SM-14Cr-0.7B. Deep etching.

Table III. EDS Microanalysis of the Martensitic Matrixes and the M₂B-Type Borides of the Spray-Formed Boron-Modified SMSS

Weight Percent	Matrix					M ₂ B			
	Pct Fe	Pct Cr	Pct Ni	Pct Mo	Pct Si	Pct Fe	Pct Cr	Pct Ni	Pct Mo
SM-0.3 pct B	80.8	11.6	6.0	1.3	0.3	56.2	30.8	1.7	11.0
SM-0.5 pct B	82.0	11.0	5.7	1.1	0.1	66.0	14.2	4.0	15.4
SM-0.7 pct B	81.7	10.7	6.1	1.0	0.4	67.1	23.8	3.0	5.8
SM-14Cr-0.7B	78.3	13.4	6.1	0.9	0.5	60.6	33.5	2.4	3.0

regions reducing the corrosion properties. Spray forming process also plays an important role on the microstructure formation, since it allows the production of alloys with extremely low levels of micro/macrosegregation, and hence with high levels of microstructural and chemical homogeneity, which may be crucial for the corrosion resistance of alloys.

The M₂B phase is a transition metal boride where M is usually rich in Fe and Cr. Therefore, it is expected that any variation of the boron content, and consequently variation of final boride fraction, may also change the final chemical composition of the martensitic matrix. Table III shows the EDS microanalysis results of both the martensitic matrix and the M₂B-type borides of the spray-formed boron-modified SMSS. It can be seen that, in all cases, the M₂B borides are Fe-rich phases containing different contents of Cr, Ni, and Mo. Although minor in comparison with Fe, the presence of these elements in the M₂B borides (mainly Cr) is far from being negligible. This means that it is reasonable to find martensitic matrixes with reduced Cr and Mo contents compared to the overall composition depicted in Table II. It must be stressed, however, that a straightforward comparison between the values given in Tables II and III is not feasible. Indeed, the local chemical compositions presented in Table III do not consider the presence of boron, whose detection is limited by EDS analysis. In addition, the composition fractions are calculated only considering the detected elements (low fraction elements are not considered), which means that the values given in Table III are forcibly overestimated. In spite of this drawback in terms of quantitative evaluation, some interesting results can be pointed out. In the case of the SM-0.5B and SM-0.7B, the remaining Cr contents of the martensitic matrixes were 11.0 and 10.7 wt pct, which is reported as the threshold content to allow passivation. On the other hand, the Cr content at the matrix of the SM-0.3B was about 11.6 wt pct, which remains within the range of conventional medium alloy SMSS grade. In the case of the SM-14Cr-0.7B, the martensitic matrix presented a Cr content still higher than the conventional high alloy SMSS grade, about 13.4 wt pct. In all cases, the remaining Mo and Ni contents of the martensitic matrixes were about 1.0 and 6.0 wt pct, respectively. It must be noticed that in the cases of the SM-0.5B and SM-0.7B, the reduction in the Cr content is uniform in the martensitic matrix, differently than the depleted Cr regions as described above for the wear-resistant tool steels after carbides precipitation.

Figure 4(a) presents the EIS results of the commercial SMSS tested using protocols I, II, and III. It can be seen

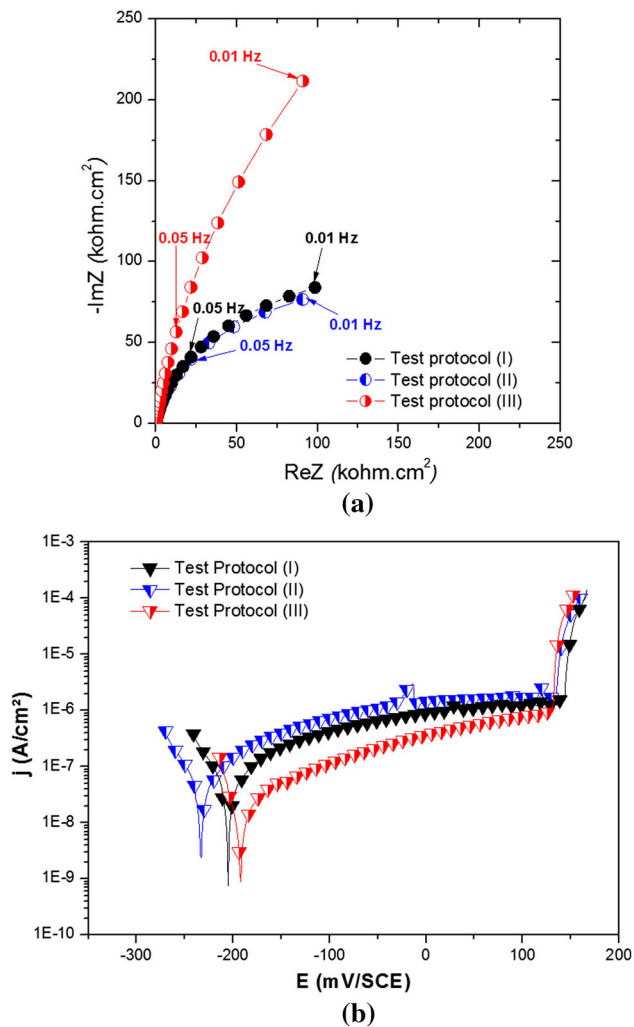


Fig. 4—(a) EIS and (b) polarization results of the commercial SMSS. Electrolyte: 35 g/L NaCl, pH 4.0.

that when the commercial SMSS is subjected to pre-passivation treatment (protocol I), and when it is maintained only one hour in solution (protocol II), the EIS results were quite similar. These results show that the pre-passivation treatment in water has practically no effect on the quality of the passive film formed on the surface of the commercial SMSS. On the other hand, when the commercial SMSS is maintained for 12 hours in the test solution (protocol III), the impedance values are considerably higher than previous two cases. Such result shows that longer immersion period under

acid-chloride media, which is considerably more oxidizing than deionized water, favors the formation of the passive film. Thus, a more protective passive film is probably formed in protocol III, resulting in higher impedance values. Figure 4(b) shows the polarization curves of the commercial SMSS after the three test protocols. One can see that all curves presented similar behavior with passive plateau and no activation peak, meaning that the passive films are present throughout the polarization tests. For the commercial SMSS, similar values of E_{corr} (around -200 mV/SCE) and E_{pit} (about 140 mV/SCE) were found regardless the test protocol. However, the corrosion current density (j_{corr}) and the current density throughout the passive plateau of the commercial SMSS subjected to protocol III were slightly lower than those observed when protocols I and II were applied (Table IV summarizes the results obtained from the ensemble of polarization curves). Such reduction of the anodic current when the samples stay longer in the test solution seems to corroborate the assumption that a more protective passive film is formed in protocol III. Nevertheless, it must be stressed that this apparent improvement of the film for samples treated according to protocol III did not correspond to an increase in the pitting potential. As shown in Figure 4(b) and in the E_{pit} values (Table IV), this better behavior is limited to the region close to the corrosion potential, while the pitting potential is roughly the same regardless the measurement protocol.

Figure 5 shows the EIS and the potentiodynamic polarization results of the different spray-formed boron-modified SMSSs after being pre-passivated for 24 hours in deionized water (protocol I). The EIS results—Figure 5(a)—show that the impedance values are similar to the commercial SMSS regardless the alloys' chemical composition. This is a quite interesting result, which shows that in less oxidizing environments or, in other words, as far as the service conditions remain close to corrosion potential conditions, all the boron-modified SMSSs show roughly the same behavior as the commercial alloy. This is confirmed by the polarization curves depicted in Figure 5(b), where it can

be seen that the different curves almost merge in the corrosion potential region with differences between their E_{corr} lower than 30 mV, and almost identical j_{corr} values,

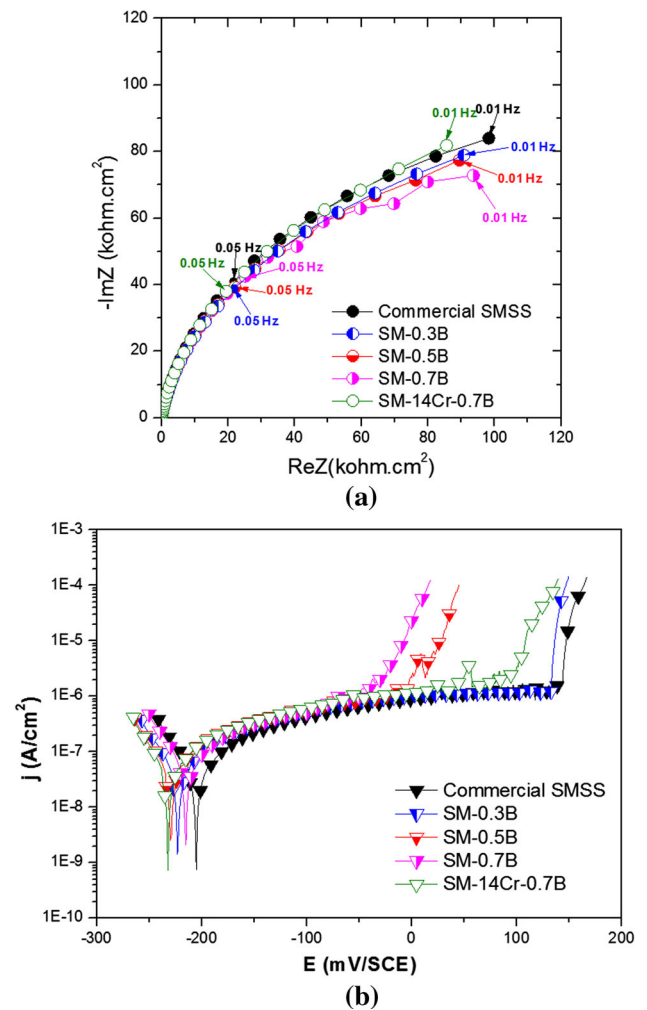


Fig. 5—(a) EIS and (b) polarization results of the spray-formed boron-modified SMSSs in protocol I.

Table IV. Mean Values of the Corrosion Properties Obtained from the Polarization Curves for the Three Test Protocols Applied

	Commercial SMSS	SM-0.3B	SM-0.5B	SM-0.7B	SM-14Cr-1B
Protocol I					
j_{corr} (A/cm ²)	4×10^{-8}	4×10^{-8}	4×10^{-8}	5×10^{-8}	4×10^{-8}
E_{corr} (mV)	-205	-220	-220	-232	-229
E_{pit} or E_{crit} (mV)	146	70	13	-19	88
$\Delta E = E_{\text{pit}} - E_{\text{corr}}$ (mV)	351	290	233	212	317
Protocol II					
j_{corr} (A/cm ²)	5×10^{-8}	9×10^{-8}	4×10^{-7}	4×10^{-7}	5×10^{-8}
E_{corr} (mV)	-240	-257	-347	-268	-165
E_{pit} or E_{crit} (mV)	146	0	-244	-102	59
$\Delta E = E_{\text{pit}} - E_{\text{corr}}$ (mV)	386	257	103	166	225
Protocol III					
j_{corr} (A/cm ²)	1×10^{-8}	2×10^{-8}	3×10^{-7}	3×10^{-7}	1×10^{-8}
E_{corr} (mV)	-182	-178	-375	-429	-189
E_{pit} or E_{crit} (mV)	136	137	-249	-297	129
$\Delta E = E_{\text{pit}} - E_{\text{corr}}$ (mV)	318	315	125	132	318

Solution: 35 g/L NaCl and pH 4.0.

as shown in Table IV. However, the E_{pit} values for the different boron-modified samples appeared to be lower than the commercial one. This was mainly the case of SM-0.5B and SM-0.7B, which presented considerably lower E_{pit} values (13 and -19 mV/SCE, respectively) when compared to the commercial SMSS (146 mV/SCE). Although lower than the commercial SMSS, the E_{pit} values of the SM-0.3B and SM-14Cr-0.7B samples (70 and 88 mV/SCE, respectively) were considerably higher than those observed for the SM-0.5B and SM-0.7B.

Figure 6 presents the EIS and polarization results of the spray-formed boron-modified SMSS carried out using protocol II. In this case, even at corrosion potential conditions, the boron-modified alloys behave differently from the commercial SMSS. The impedance values of the SM-0.3B and SM-14Cr-0.7B—Figure 6(a)—were lower than those observed for the commercial SMSS. Their respective polarization curves—Figure 6(b)—indicate that the behavior presented by the SM-0.3B and SM-14Cr-0.7B tended to the one shown by the commercial SMSS. Both alloys showed low j_{corr} (9×10^{-8} A/cm² and 5×10^{-8} A/cm²,

respectively) and formation of passive plateau. However, the length of the passive plateau which can be estimated as $\Delta E = E_{\text{pit}} - E_{\text{corr}}$ was considerably shorter when compared to the commercial SMSS (see Table IV). This set of results shows that the passive films formed on the SM-0.3B and SM-14Cr-0.7B surfaces after one hour of OCP are less protective, probably thinner and/or less uniform, than the passive film formed on the commercial SMSS surface under the same conditions. On the other hand, the SM-0.5B and SM-0.7B showed considerably higher j_{corr} than the other alloys (about 4×10^{-7} A cm⁻²), followed by an increase in the anodic current up to 0.1 mA cm⁻² without presenting passive plateau. Accordingly, the EIS results showed smaller loops, which are consistent with the absence of passivating plateau and an activation-like kinetic evolution of the metal-electrolyte interface as the overpotential increases.

Figure 7 presents the results of the analysis carried out using the test protocol III. The EIS results—Figure 7(a)—show that when the SM-0.3B and SM-14Cr-0.7B stay longer in the acid-chloride solution, their impedance values are quite similar to that observed

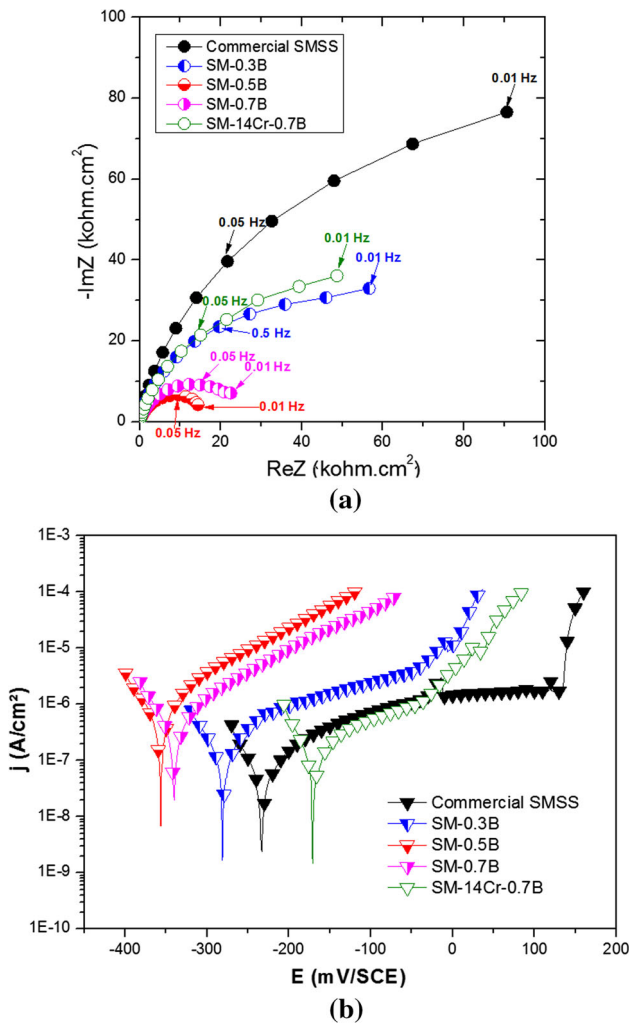


Fig. 6—(a) EIS and (b) polarization results of the spray-formed boron-modified SMSSs in protocol II.

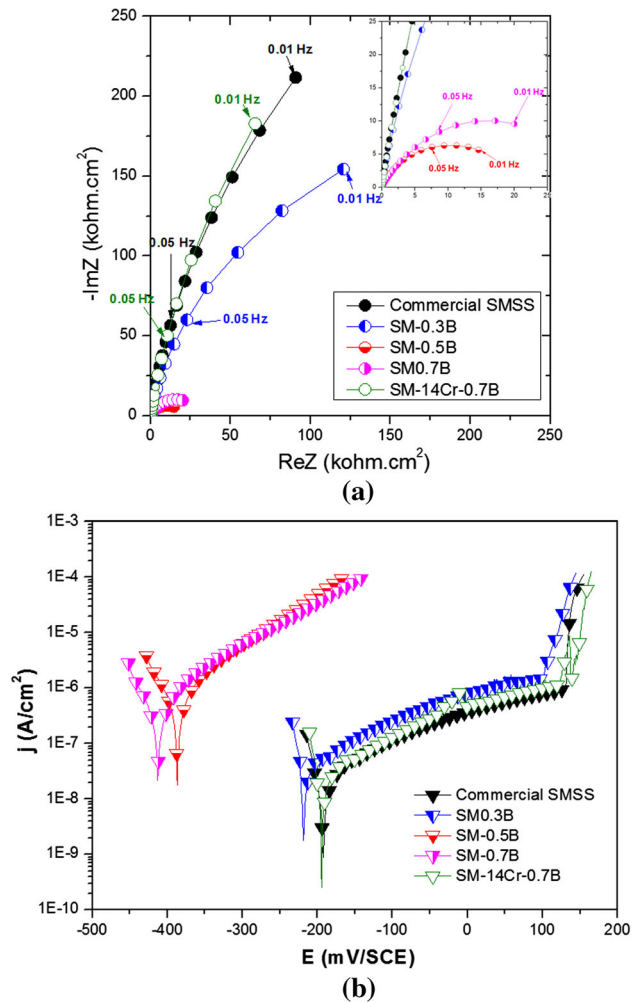


Fig. 7—(a) EIS and (b) polarization results of the spray-formed boron-modified SMSSs in protocol III.

for the commercial SMSS. The same can be seen in the polarization curves—Figure 7(b). When the SM-0.3B and SM-14Cr-0.7B stay longer in the acid-chloride solution, their corrosion behaviors are similar to that presented by the commercial SMSS. The E_{corr} , E_{pit} and j_{corr} are practically the same (Table IV). Such results make clear that the SM-0.3B and SM-14Cr-0.7B need longer immersion periods in the acid-chloride solution, when compared to the commercial SMSS, to form a stable and uniform passive film. However, if sufficient time is given, the corrosion properties of these two spray-formed boron-modified SMSS no longer differ from the commercial SMSS. Meanwhile, the EIS and potentiodynamic polarization results of the SM-0.5B and SM-0.7B are virtually the same when the protocols II and III are applied. Since both alloys are not able to passivate in such acid-chloride media, they undergo generalized corrosion with the corrosion rate being given by j_{corr} .

Based on the electrochemical analysis, it can be argued that in the case of the spray-formed boron-modified SMSS grades, the chemical composition of the alloys plays the central role on their corrosion behavior. The results show that the formation of the M_2B -type borides reduces the overall Cr content in the martensitic matrix. EIS and polarization results show that the chemical composition of the final martensitic matrixes determines the alloys corrosion resistance. When immersed in the acid-chloride media, the SM-0.5B and SM-0.7B, which have the residual Cr content in the matrixes below the threshold value of stainless steel grades (about 11 wt pct), did not present passivation and behave as an active metal, presenting generalized corrosion during polarization. On the other hand, the SM-0.3B and SM-14Cr-0.7B, whose matrixes presented Cr contents above 11 wt pct (11.6 and 13.4 wt pct, respectively), when immersed for longer periods in the acid-chloride media, behave quite similar to the commercial SMSS. The test protocol III showed that both alloys (SM-0.3B and SM-14Cr-0.7B) are able to passivate in the more aggressive media presenting similar corrosion properties as that of the commercial SMSS.

Figure 8 shows the corroded surfaces of the commercial SMSS and the spray-formed boron-modified SMSSs after being anodically polarized until a current density of 5 mA cm^{-2} . The similarity of the corrosion behavior of the SM-0.3B and SM-14Cr-0.7B when compared to the commercial SMSS can be observed in their corroded surfaces presented in Figures 8(a), (b) and (e), which clearly show that these alloys suffered localized corrosion by pits, which present approximately the same size. Since the SM-0.3B and SM-14Cr-0.7B showed that they are able to passivate in the acid-chloride media used, the polished samples were immersed for 12 hours in solution before being polarized (as in test protocol III). As shown in Figure 8(b) and (e), the polarization induced the nucleation of pits that grew deeply and confined all the anodic current, while the outer surface around remained clearly passive. A detailed image of the pit formed on the surface of the SM-14Cr-0.7B is shown in Figure 8(f). This image clearly shows that the pit grew by consuming the martensitic matrix, while the

M_2B -type borides network remained intact. These results indicate that the borides, in such test condition, have higher corrosion resistance than the steel matrixes and, therefore, the corrosion process takes place preferentially in the martensitic matrixes. On the other hand, since it was shown that the SM-0.5B and SM-0.7B are not able to passivate in the acid-chloride media, these samples were left only one hour in OCP before polarization. The corroded surfaces of both alloys are presented in Figure 8(c) and (d). In both cases, unlikely to the previous passivated samples, a more uniform corrosion is observed revealing the distribution of the boride network. In Figure 8(d), the cathodic and anodic regions are clearly seen on the corroded surface of the SM-0.7B. It can be seen that in the anodic regions, the corrosion did not take place by forming pits, but corroding the surface in a less localized process. This may be resulted from the fact of this sample be unable to develop a protective passive film in such acid-chloride solution. Again, the corrosion process in the anodic regions seems to preferentially occur in the martensitic matrixes with the M_2B -type borides apparently remaining inert at the grain boundaries.

The corroded surfaces presented in Figure 8 show that the martensitic matrixes are the microstructural features that control the corrosion process, while the borides network seems to be inert. This is clearly seen in the pit of the corroded of the SM-14Cr-0.7B, where martensitic matrixes were corroded and the borides network remained apparently intact.

The results so far show that SM-0.3B and SM-14Cr-0.7B present corrosion resistance similar to that of the commercial SMSS when the samples are subjected to a long resting protocol. Immersion in the acidic chloride media for a longer period allows the passive films to be strengthened, increasing their corrosion protection efficiency. The need of using longer immersion periods for the spray-formed boron-modified SMSSs in order to form a protective passive film, raises the question about how the presence of borides affect the passivation kinetics of the alloy. Boron-modified SMSS grades were developed to be applicable under severe wear and corrosive environment conditions. This means that in service conditions, the passive film is prone to be often locally damaged by different mechanical loads, impacts, fretting, and so on, involving different wear mechanisms. In these situations, the kinetic of repassivation of the surface is a crucial issue. Based on this, EN measurements were performed to evaluate the repassivation kinetics of the SM-0.3B and SM-14Cr-0.7B compared to that of the commercial SMSS after a simulated abrasion event imposed upon the surface of the sample connected to the CE terminal. Figure 9 presents the coupling current between the identical samples recorded before and after abrasion. Before abrasion, the samples were maintained for 24 hours immersed in the solution aiming to have all surfaces covered by a long-aged passive film, which would result in near-zero coupling current values. Low coupling currents were effectively observed before abrasion as shown by the black curves in Figure 9. After the abrasion event, the abraded CE surface (damaged

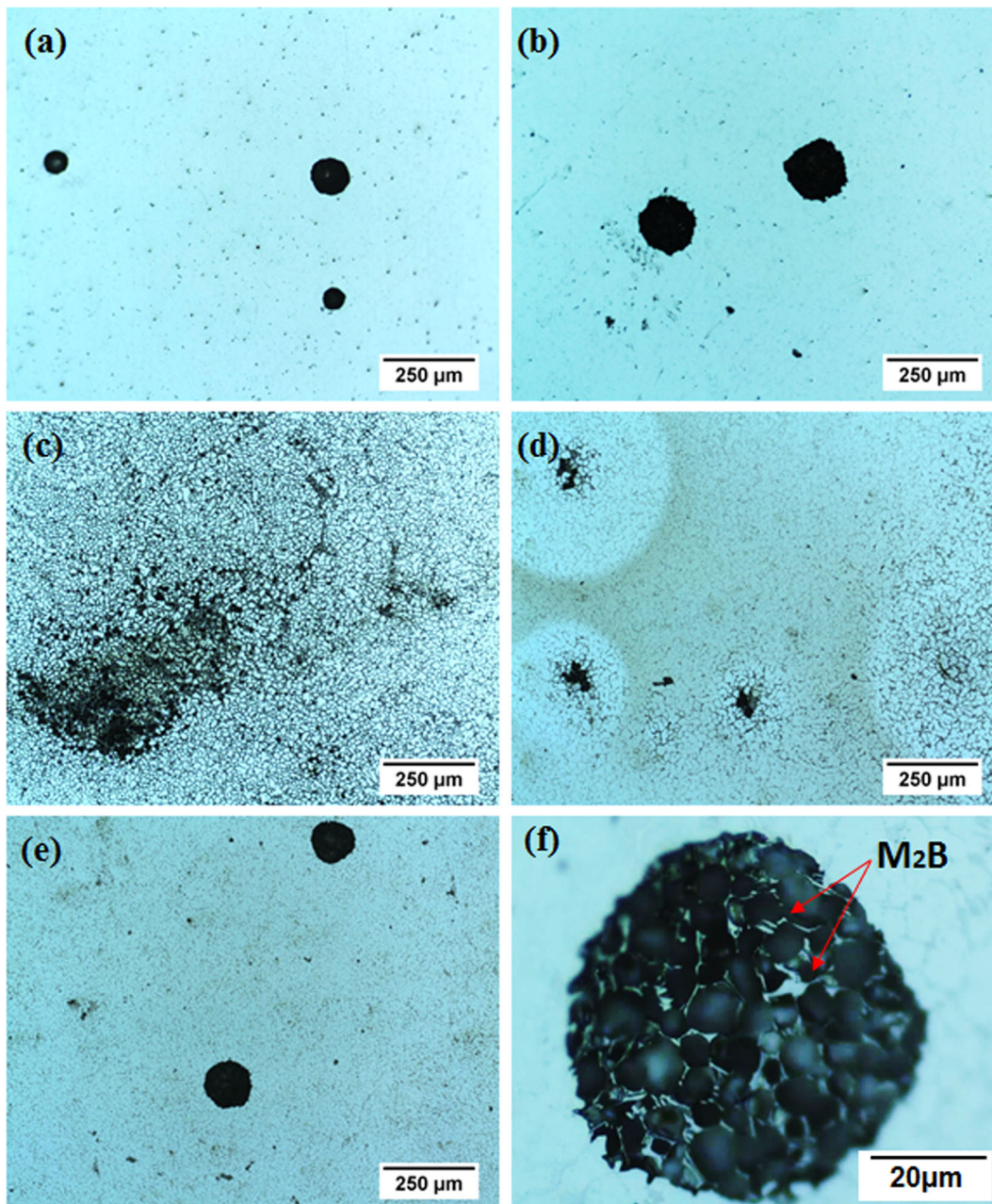


Fig. 8—Corroded surfaces of (a) commercial SMSS (b) SM-0.3B, (c) SM-0.5B, (d) SM-0.7B, (e) SM-14Cr-0.7B, and (f) zoom showing the intact M_2B network within a pit of the SM-14Cr-0.7B.

passive film) should behave anodically, while the intact WE should behave cathodically, delivering a negative sign current flow to be sensed by the ZRA. It can be seen that in all cases immediately after abrasion, the recorded currents were negative and as high as 10^{-6} A in absolute values. Such currents result from the oxidation reactions taking place on the surface of the abraded samples resulting in their repassivation. With the repassivation process, the currents decrease along the time until recovering low current values (near zero), indicating that both surfaces are almost identical again.

Two different approaches were used to comparatively evaluate the repassivation kinetics of the alloys. First, the

time for the coupling current to reach 10 pct of the maximum recorded current was determined for each alloy. Figure 10 (a) shows the time evolution of the normalized current (regarding the maximum current). It can be seen that the commercial SMSS reaches 10 pct of the maximum current (represented by the dashed red line at $I/I_{\max} = 0.1$) in only 8.1 seconds, whereas the SM-0.3B and SM-14Cr-0.7B took 51.6 and 184.4 seconds, respectively. These results show that the current recovery of the commercial SMSS is considerably faster than the SM-0.3B and SM-14Cr-0.7B. In spite of different kinetics, it is important to observe that all the samples showed an effective repassivation process after film damage.

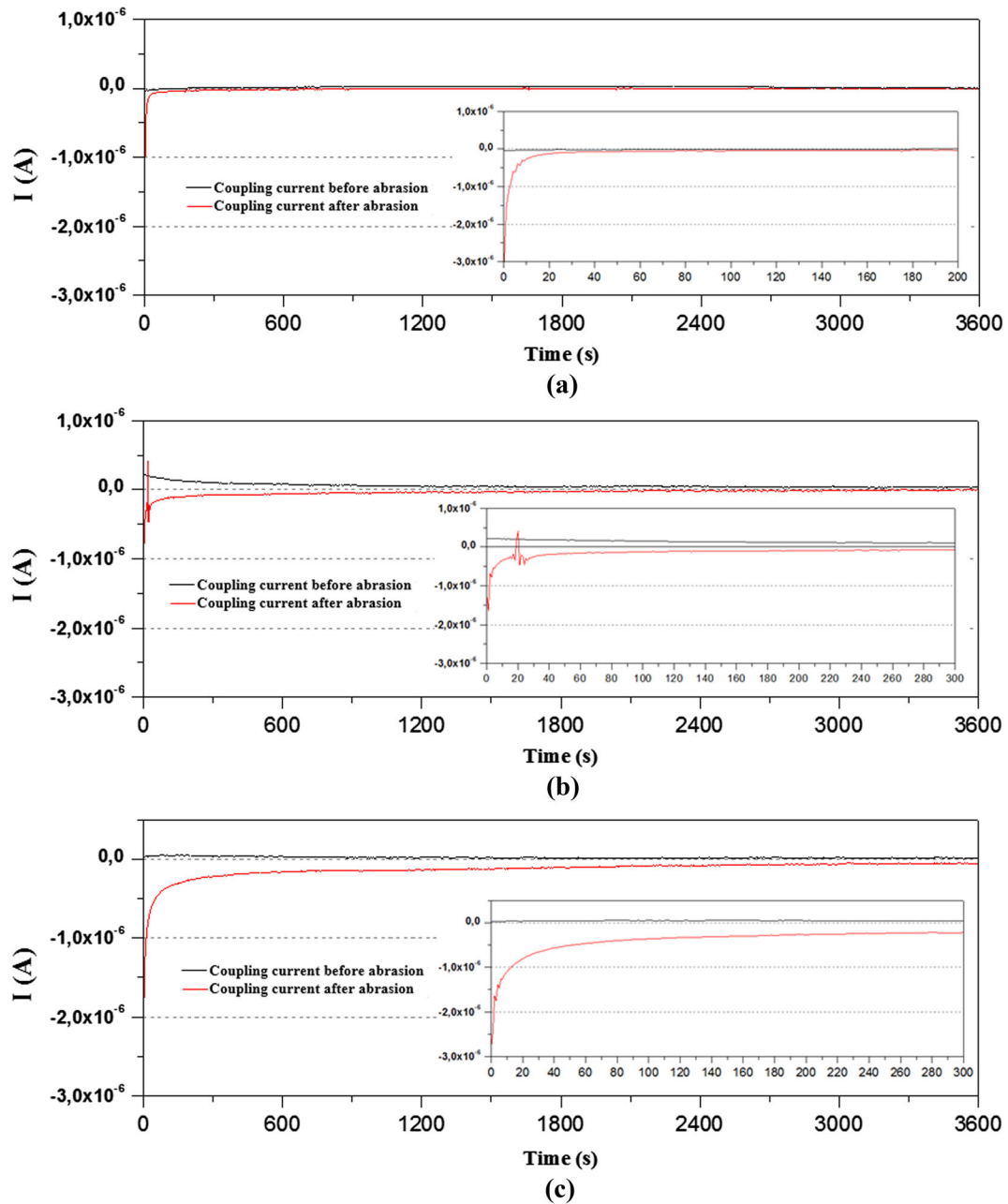
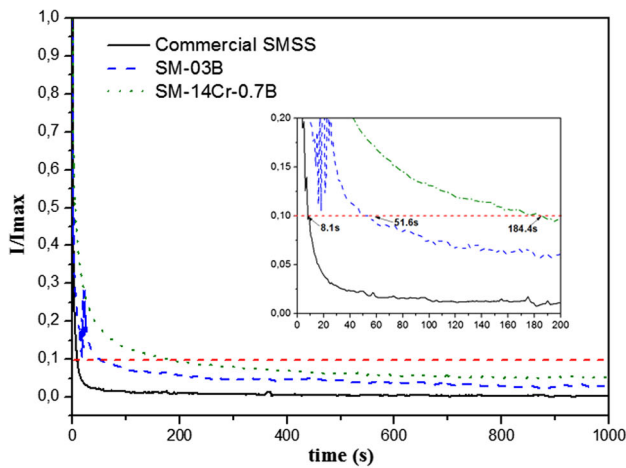


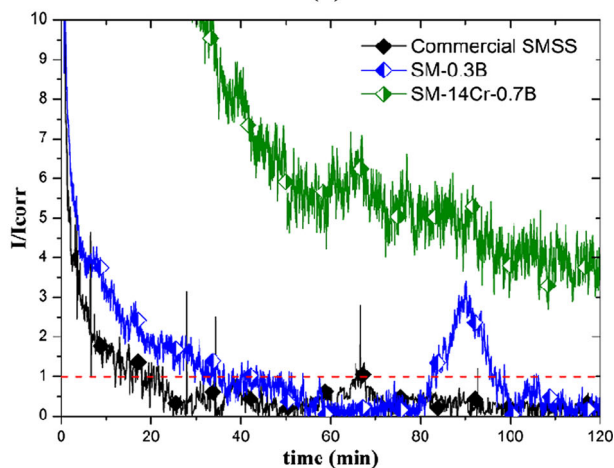
Fig. 9—Coupling currents measured by EN before and after abrasion of (a) commercial SMSS, (b) SM-0.3B, and (c) SM-0.7B. Arbitrary zero time origin.

The second approach was to determine the time taken by the current to recover the I_{CORR} determined by the polarization curves of the corresponding samples, when the test protocol III was applied (Table IV). Figure 10(b) presents the I/I_{CORR} vs time behavior for the three alloys. It can be seen that in about 18 min, the I_{CORR} of the commercial SMSS was reached, meaning that, after this time, the condition before the abrasion was practically restored. In the case of the SM-0.3B, the time taken to restore the corrosion current was around 32 minutes, whereas in the case of the SM-14Cr-0.7B, even after 2 hours, the current was still 3 times higher than the previously measured I_{CORR} .

As expected, the EN measurements showed that the coupling current of the commercial SMSS, after a simulated abrasion event, decreased considerably faster than the SM-0.3B and SM-14Cr-0.7B. However, the repassivation kinetics of the SM-0.3B was unexpectedly faster than the SM-14Cr-0.7B, even the first one having lower remaining Cr content in the martensitic matrix. A possible reason is that higher the boride fraction, the more discontinuous is the oxide layer initially formed both in terms of film coverage and thickness. In these conditions, the simulated abrasive event would have a deeper impact on the surface exposure for the SM-14Cr-0.7B, hence yielding a slightly slower



(a)



(b)

Fig. 10—(a) I/I_{max} and (b) I/I_{corr} measured by EN.

repassivation kinetics compared to the more homogeneous SM-0.3B passive film. This result suggests that the boride fraction (when the minimum chromium content to guarantee the passivation of the matrix is present) may have an important influence on the repassivation kinetics of the boron-modified stainless steels. Deeper studies involving corrosion mechanisms and corrosion products analyses must be carried out to understand how the presence of borides and the boride fraction affect the passivation mechanisms of this sort of alloy. However, this studied is beyond the scope of this work.

In any case, the most important result was to show that the SM-0.3B and SM-14Cr-0.7B are able to repassivate after a wear event in the acid-chloride media. The results demonstrate that if the Cr content of the spray-formed boron-modified SMSS grades, regardless of the boron content, is controlled in such a way that the Cr content of the martensitic matrix remains within the range of the conventional commercial SMSS grades, the corrosion resistance of the alloy may not be considerably impaired. This is a quite encouraging result, since addition of alloying elements to form or precipitate second phases aiming at increasing the hardness and/or wear resistance may be

accompanied by a substantial reduction of the corrosion properties.

IV. CONCLUSIONS

The electrochemical corrosion behavior of four compositions of spray-formed boron-modified SMSS was evaluated. It could be concluded that once the Cr content of the martensitic matrix remains above 11 wt pct, the results show that the spray-formed boron-modified SMSS grades behave similar to the commercial SMSS in acid-chloride media, regardless of the boron content. When the chromium content of the martensitic matrix is sufficient to guarantee the passivation, the difference between the spray-formed boron-modified SMSS grades and the commercial SMSS lies in the repassivation kinetics, which is slower when the M_2B -type borides are present in the microstructure.

REFERENCES

1. J. J. Dufrane: in *Supermartensitic Stainless Steels 99*, Brussels, Belgium, 1999, pp. 19–24.
2. P. Toussaint, and J. J. Dufrane: in *Supermartensitic Stainless Steel 2002*, Brussels, Belgium, 2002.
3. C.A. Della Rovere, C.R. Ribeiro, R. Silva, L.F.S. Baroni, N.G. Alcântara, and S.E. Kuri: *Mater. Sci. Eng. A*, 2013, vol. 586, pp. 86–92.
4. Y. Kondo, K., Ueda, M., Ogawa, K., Amaya, H., Hirata, H., Takabe, and H., Miyazaki: in *Supermartensitic Stainless Steels 99*, Brussels, Belgium, 1999, pp. 11–18.
5. G.Y. Koga, R.P. Nogueira, V. Roche, A.R. Yavari, A.K. Melle, J. Gallego, C. Bolfarini, C.S. Kiminami, and W.J. Botta: *Surf. Coatings Technol.*, 2014, vol. 254, pp. 238–43.
6. P. Sharma and J.D. Majumdar: *Metall. Mater. Trans. A*, 2015, vol. 46A, pp. 3157–65.
7. D.J. Branagan, W.D. Swank, D.C. Haggard, and J.R. Fincke: *Metall. Mater. Trans. A*, 2001, vol. 32A, pp. 2615–21.
8. S.H.C. Park, Y.S. Sato, H. Kokawa, K. Okamoto, S. Hirano, and M. Inagaki: *Metall. Mater. Trans. A*, 2009, vol. 40A, pp. 625–636.
9. C.-K. Fang and T.H. Chuang: *Metall. Mater. Trans. A*, 1999, vol. 30A, pp. 941–48.
10. T. Zhang and D.Y. Li: *Metall. Mater. Trans. A*, 2002, vol. 33A, pp. 1981–89.
11. G. Zepon, C.S. Kiminami, W.J. Botta, and C. Bolfarini: *Mater. Res. J. Mater.*, 2013, vol. 16, pp. 642–46.
12. C.-N. Chang and F.-S. Chen: *Mater. Chem. Phys.*, 2003, vol. 82, pp. 281–87.
13. G. Abbas, and U. Ghazanfar: *20th ICALEO 2001, Vols 92 93, Congr. Proc.*, 2001, pp. 679–84.
14. D.H. Nam, K. Lee, and S. Lee: *Metall. Mater. Trans. A*, 2007, vol. 38A, pp. 1193–1201.
15. G. Zepon, A.R.C. Nascimento, A.H. Kasama, R.P. Nogueira, C.S. Kiminami, W.J. Botta, and C. Bolfarini: *Mater. Des.*, 2015, vol. 83, pp. 214–23.
16. A. Basak, D.K. Roy, and G.L. Dutta: *Wear*, 1995, vol. 184, pp. 241–44.
17. D. Uzunsay: *Mater. Des.*, 2010, vol. 31, pp. 3896–3900.
18. T. Singh and G. Sundararajan: *Metall. Mater. Trans. A*, 1990, vol. 21, pp. 3187–99.
19. G. Straffelini, A. Molinari, and D. Trabucco: *Metall. Mater. Trans. A*, 2002, vol. 33A, pp. 613–24.
20. N. Yüksel and S. Şahin: *Mater. Des.*, 2014, vol. 58, pp. 491–98.
21. A. Schulz, V. Uhlenwinkel, C. Escher, R. Kohlmann, A. Kulmburg, M.C. Montero, R. Rabitsch, W. Schützenhöfer, D. Stocchi, and D. Viale: *Mater. Sci. Eng. A*, 2008, vol. 477, pp. 69–79.

22. D.M. Goudar, K. Raju, V.C. Srivastava, and G.B. Rudrakshi: *Mater. Des.*, 2013, vol. 47, pp. 489–96.
23. D.M. Goudar, K. Raju, V.C. Srivastava, and G.B. Rudrakshi: *Mater. Des.*, 2013, vol. 51, pp. 383–90.
24. A.H. Kasama, A.J. Mourisco, C.S. Kiminami, W.J. Botta, and C. Bolfarini: *Mater. Sci. Eng. A*, 2004, vols. 375–377, pp. 589–94.
25. T.T. Matsuo, C.S. Kiminami, W.J. Botta, and C. Bolfarini: *Wear*, 2005, vol. 259, pp. 445–52.
26. V.C. Srivastava, G.B. Rudrakshi, V. Uhlenwinkel, and S.N. Ojha: *J. Mater. Sci.*, 2009, vol. 44, pp. 2288–99.
27. T.A. Adler and R.P. Walters: *Corros. Sci.*, 1992, vol. 33, pp. 1855–76.
28. G. Zepon, N. Ellendt, V. Uhlenwinkel, and C. Bolfarini: *Metall. Mater. Trans. A*, 2016, vol. 47A, pp. 842–51.
29. N.J. Calos, E. Graham, D.R. Cousens, P. Christodoulou, C.H.L. Kennard, L.K. Bekessy, and S.F. Parker: *Mater. Trans.*, 2001, vol. 42, pp. 496–501.
30. P.E. Busby, M.E. Warga, and C. Wells: *Trans. Am. Inst. Min. Metall. Eng.*, 1953, vol. 197, pp. 1463–68.
31. R.A. Mesquita and C.A. Barbosa: *Mater. Sci. Eng. A*, 2004, vol. 383, pp. 87–95.